Development of a Magnetic Camera for Barcode and QR Magnetic Identification Tag Readout

Alberto Nicolicea
alberto.nicolicea@tecnico.ulisboa.pt

Instituto Superior Técnico, Lisboa, Portugal

December 2021

Abstract

QR Codes have gained popularity in recent years and are very used nowadays in commercial activities. The current technology for detection employed is based on optical devices. The novel idea of developing a QR Code reader based on TMR sensors is explored in this thesis in order to read codes printed with magnetic ink.In order to achieve this, simulations are produced in order to study the effect of the reading distance and magnetization detection on the QR Code mapping. A system is then proposed, consisting of layered sensor stack, together with the corresponding multiplexing and amplification electronics. The system was then fabricated, assembled and the sensors are tested and characterized.Due to the lack of time, a final functional product was not achieved within the time-frame of the thesis.However, the concept was proved and functional sensors were produced.
Keywords: QR Codes, Magnetic Ink, Magnetic Tunnel Junctions, Magnetic Camera, 2D Magnetic Pattern Simulation

1. Introduction

QR Code - Quick Response Code - is a two-dimensional, machine-readable, matrix barcode where data is encoded in both vertical and horizontal directions in the form of an image, consisting of black and white modules which represent the encoded data. It is the most popular 2D barcode commercially used. Matrix Codes or 2D Barcodes are analogous to 1D barcodes [1], with the advantage of storing a much larger ammount of information, proportional to the surface instead of the length as in the one-dimensional case. [2]

QR Codes have widespread applications nowadays, such as product tracking, item identification,time tracking, transport ticketing, document management and general marketing. [3]

The objective of this project is the development of a magnetic camera constituted by a matrix of magnetoresistive sensors, with the objective of scanning magnetic barcodes and QR codes, developing and optimizing the multiplexing electronics system and the user interface and testing on samples in the laboratory.

2. Theoretical Background and Simulations

At a large enough distance from a magnetic dipole, it can be considered punctual, which the magnetic potential being given by:

$$\psi(\vec{r}) = \frac{\vec{m} \times \vec{r}}{4\pi r^3} \tag{1}$$

The resulting magnetic field created by each pixel at a position vector $\vec{r}$ relative to it is given by: ([4],[5])

$$\vec{H} = -\Delta\psi = \frac{1}{4\pi}\left[\frac{3\vec{r}(\vec{r}\cdot\vec{m})}{r^5} - \frac{\vec{m}}{r^3}\right] \qquad (A/m) \tag{2}$$

- $\vec{m}(A \cdot m^2)$ - Finite Element Magnetic Moment
  r - Finite Element Distance (m)

Using this long-range dipole model, simulations of the 2D magnetic field mapping produced by QR Codes printed in magnetic ink can be obtained.

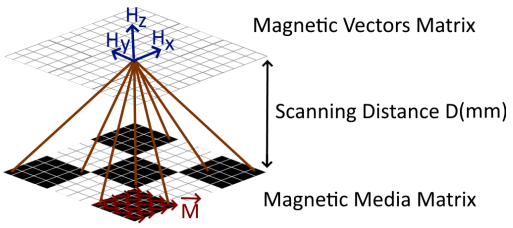

Figure 1: Finite Elements Method used for the calculation of the Magnetic Field Mapping of Magnetic QR Patterns

The finite elements method is used. The schematic of this method is shown above. A matrix containing the magnetic pattern of the QR Code is created, with each pixel consisting of a certain number of smaller magnetic dipole elements with a certain magnetization vector $\vec{M}$.

Another matrix is created at a certain simulated measuring distance $D(mm)$. Each point in this new matrix adds the contribution of all the finite elements of the matrix beneath.

This method thus sums all the contributions of all the finite elements contained in each pixels of the QR Code, so it accurately reproduces the interference between different pixels. It also does not treat each pixel as an entire dipole, but as a quasi-continuous media that contains smaller magnetic domains (finite elements).

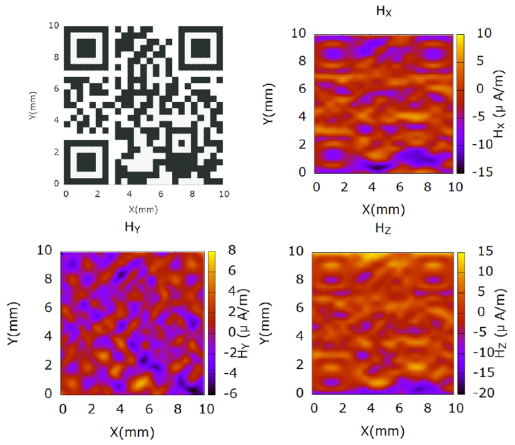

Figure 2: Mapping of the field components H_X,H_Y,H_Z Obtained for Magnetization along the X direction ($10 \times 10mm^2$pattern, $D = 0.5mm$ scanning distance)

A plot of the results obtained is shown above, with magnetization along the X axis. It can be observed that H_X corresponds to the mapping of the bulk of the pixels, H_Y corresponds to the mapping of the corners of the pixels, and the perpendicular H_Z mapping corresponds to the mapping of the edges of the pixels.

From a practical point of view, if the sensors were reading the field parallel to the magnetization X, they would be saturated by the permanent magnets and would not be able to read the field emitted for the sample. Reading the component in Y would also not provide valuable information since it is a mapping of the corners of the pixels. Therefore the only component worth considering for practical purposed is the component H_Z of the magnetic field perpendicular to the plane of magnetization. This was the reading mode used for the experimental work.

Since the magnetic component perpendicular to the magnetization gives information about the edges of the pixels, an algorithm needs to be employed to reconstruct the bulk or body of the pixels. The method is shown above, consisting of 3 mains steps and 1 final error calculation step.

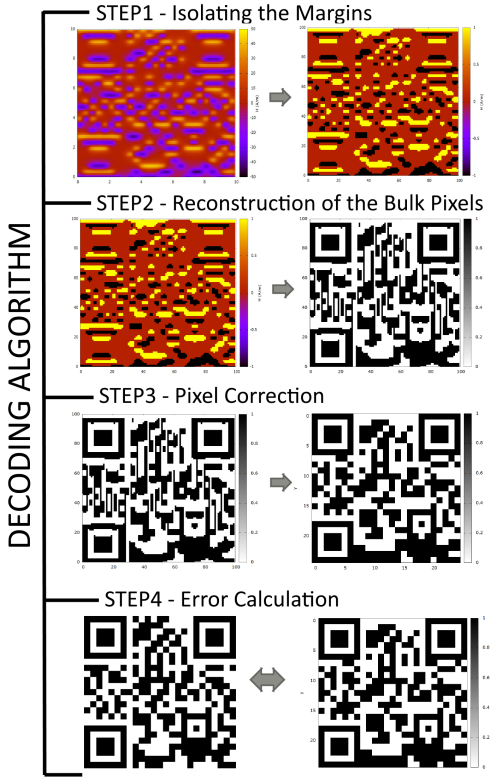

Figure 3: Schematic of the Pixel decoding algorithm

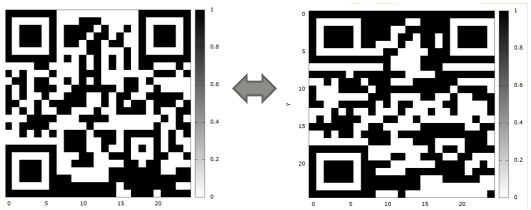

Figure 4: Simulated reconstructed QR - Left, Experimental reconstructed QR from Simulations- Right

This method was applied to simulations and to results obtained experimentally using a scanner present at INESC-MN that employed TMR sensors. A QR code was thus reconstructed from both source and compared, as shown above.

A table with the comparison of the experimental error is shown beneath. It can be seen that the error is bellow the 30% which is the maximum error threshold reconstruction capacity of the Solomon Algorithm in both cases.

Simulated Error	Experimental Error	Threshold Error
10%	24.96%	30%

Table 1: Error Comparison between experimental measurements and simulations

In the figure above it can be seen that for the case of a 10x10mm QR Code, only at mea-

suring distances of $D = 0.2mm$ and bellow is it possible to distinguish the QR Code pixels properly. Hence, the recommended ratio between the measuring distance and QR Code width W should be no larger than $\frac{D}{W} = 0.02$ (2%). For this reason, reducing the size of the QR code is limited by the practicality of reducing the measuring distance for actual measurements.

Based on this it is possible to build a table with the maximum recommended measurement distances as a function of the QR Code dimensions, for the Version2 with 25x25 pixels:

QR Dimensions	Recomm. Max. Scan Dist.
$10cm \times 10cm$	2 mm
$1cm \times 1cm$	0.2 mm
$1mm \times 1mm$	0.02 mm

Table 2: Recommended maximum measuring distances

For example, for a realistic measuring distance of $D = 0.5mm$, a QR code (Version 2) with at least $2.5cm \times 2.5cm$ is needed in order to be possible to properly to distinguish individual pixels.

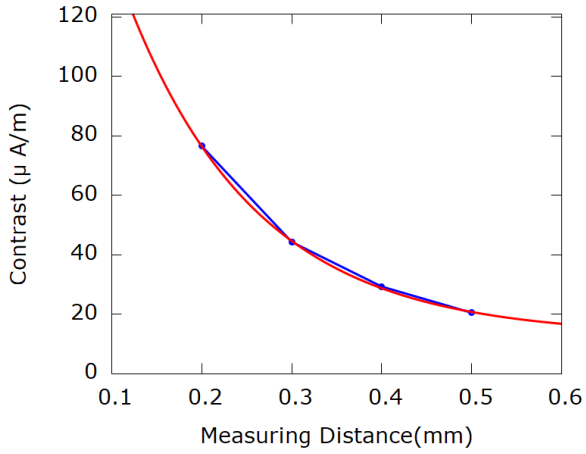

Figure 5: Contrast of the Mapping as a function of the detection distance: Quadratic fitting (Left) and Third Power Fitting (Right)

A plot of the contrast of the mapping as a function of the measuring distance is shown in figure 5. The following negative exponential model was used:

$$f(x) = a \cdot exp(-b \cdot x) + c \tag{3}$$

The parameters for the negative exponential fitting are given in table 3.

Parameter	a($\mu A/m$)	b(mm^{-1})	c($\mu A/m$)
Value	254 ± 19	6.9 ± 0.5	12.8 ± 1.8

Table 3: Fitting parameters

3. Methodology

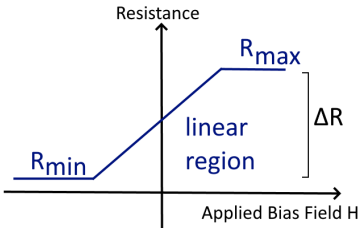

Figure 6: Ideal Magnetoresistive Linear Transfer Curve

Magnetoresistive sensors are sensors that detect an external magnetic field trough a change in their magnetoresistance (MR), as shown in the figure 6. This parameter is defined as:

$$MR[\%] = \frac{\Delta R}{R_{min}} \times 100 \tag{4}$$

Magnetoresistive Sensors are generally constituted by two ferromagnetic layers separated by a thin oxide layer, as shown in figure 7. One of the layers is a hard magnet and maintains a fixed magnetization. The other layer is a soft magnet that aligns itself with the external bias field. The relative orientation of the magnetization between these two layers determines the resistance of the junction. When the alignment is parallel, the resistance reaches a minimum. When the alignment is antiparallel, the resistance reaches a maximum. [6]

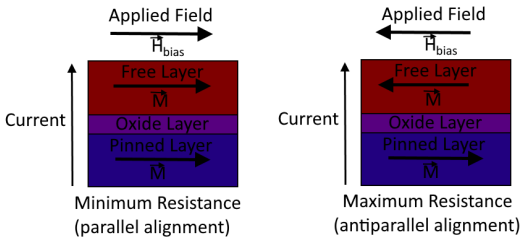

Figure 7: General Functionality of a typical TMR Junction

TMR (Tunneling Magnetoresistive) sensors are the most sensible and have the highest percentage of magnetoresistance of the order of 175%. Hence these will be the type of sensors used in this thesis, since the magnetic fields produced by magnetic ink are very weak, and the highest possible magnetoresistance is required for detection. [7]

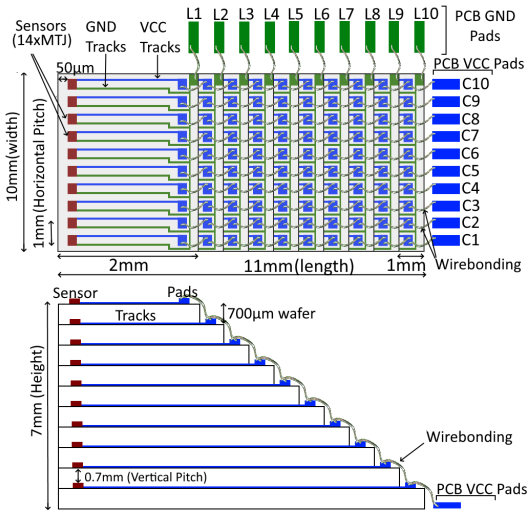

Figure 8: Sensor Setup (Top and Side View)

Based on this technology, a sensor matrix of 10x10 MTJ (Magnetic Tunnel Junction) sensors was developed, with the architecture shown in figure 8. The sensors layers were stacked upon each other. The 10 layers containing 10 sensors each thus formed a 10 by 10 sensor matrix. The sensor was fabricated in 20 different nano-fabrication steps within the clean-room environment.

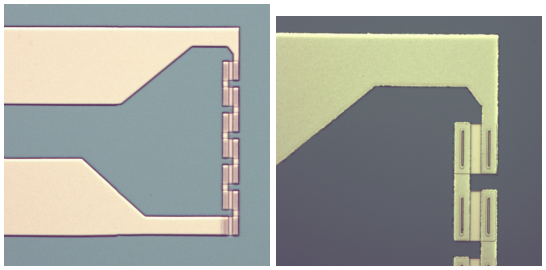

Figure 9: Sensor Overview (Left) and Junctions Overview (Right)

A microscope overview of the individual sensors constituted of 14 MTJ (Magnetic Tunnel Junctions) is shown in figure 9.

The structure and design of the fabricated magnetoresistive sensors is described in the following subsections.

3.1. MTJ Stack

The MTJ junctions fabricated are constituted by various levels, as shown in the figure above. In order to define the pillars, etching at 60º is to be done reaching the level of the oxide layer of the stack, and then etching at 30º is to be done further, up to 600Å. The bottom is to be defined using etching at 45º up to a depth of 600Å, such as to reach the isolating oxide layer present on the wafer beneath the stack.

Thus a system is formed, by which current enters trough one of the pillars, is transferred to another pillar after traversing the oxide layer beneath

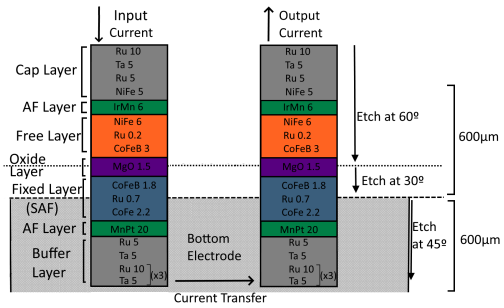

Figure 10: Sensor Design Overview

the free and fixed layers, and exits in the same way. The relative orientation between the free layers and the fixed layers in each pillar induced by external magnetic fields affects the output current, thus resulting in detection.

The MTJ Stack used was the following (units in nm):

[(Ta5/Ru10)x3/Ta 5/Ru 5/MnPt 20/Co80Fe20 2.2/Ru 0.7/ CoFeB 1.8/ MgO 1.5/ CoFeB 3/ Ru 0.2/ NiFe 6/ IrMn 6 / NiFe 5/ Ru 5/ Ta5 / Ru 10]

The expected results of CIPT after annealing are: $RA \sim 2.42kOhm$ and $TMR \sim 175\%$.

The sensor is constituted by 14 MTJ Junctions with dimensions $A_j = 20 \times 2\mu m^2$, resulting in a total sensing area of $A_s = 220 \times 21\mu m^2$, with a pole-pitch of $PP = 780\mu m$ between the sensors, as shown in the figure above. The constant resistivity$\times$area of the MTJ stack used is of $RA = 2.38k\Omega \times \mu m^2$, resulting in a total resistance of $R = 4.25k\Omega$ per sensor.

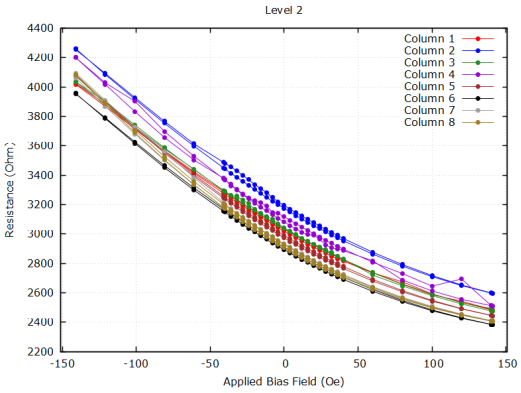

Figure 11: Magnetoresistance as a Function of the Applied Field for one of the functioning levels

Due to nanofabrication errors, only 4 of the 10 stacked levels had functional sensors. However, within the layers that had functional levels, the sensors presented a good and linear transfer curve when characterized, with good values of sensibility(S), base resistance (R_0) and coercivity(H_C), as shown in the following table:

The sensors also presented large values of magnetoresistance, of the order of $MR \approx 100 - 120\%$,

Lvl	R_0(Ohm)	S(Ohm/Oe)	H_C(Oe)
2	3 028	5.73 ± 0.12	0.96
4	2 868	5.72 ± 0.15	1.00
6	2 498	5.01 ± 0.14	1.09
9	2 920	6.36 ± 0.20	1.06
Avg	2 829	5.71 ± 0.31	1.03

Table 4: Sensibility, Coercivity and Resistance Measurements - MTJ Sensors

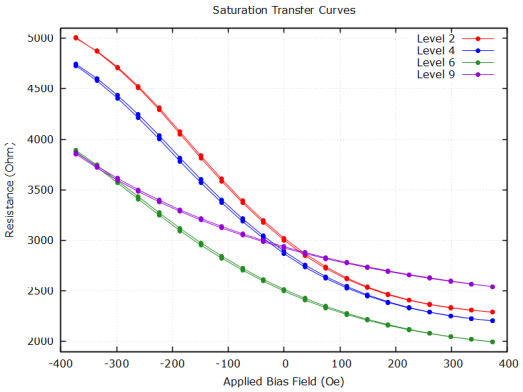

Figure 12: Magnetoresistance as a Function of the Applied Field for the 4 levels using the auto-prober

as shown in the table 5. However, these values were not close to the expected value of 175% for the TMR stack used.

Lvl	$Rmin(\Omega)$	$Rmax(\Omega)$	$\Delta R(\Omega)$	MR(%)
2	2 290	5 005	2 715	118.6
4	2 203	4 743	2 540	115.3
6	1 995	3 889	1 894	94.9
9	2 543	3 866	1 324	52.1
Avg	2 257	4 380	2 118	95.2

Table 5: Magnetoresistance Measurements - MTJ Sensors

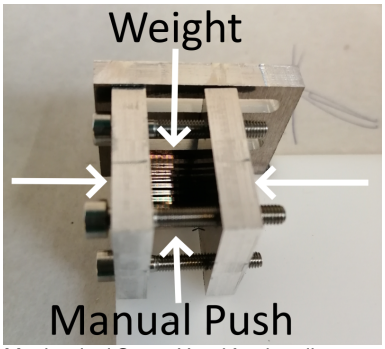

Figure 13: Mechanical Setup Used for the alignment of the sensors

Afterwards, the final sample aligned using the mechanical setup (fig. 13) and the electrical test setup that was aligned manually were inspected under microscope. A comparison between the alignment using the manual and mechanical methods are shown in figure 14 and 15. The miss-alignment presented is of each level relative to the level above it, with level 10 being the bottom level.

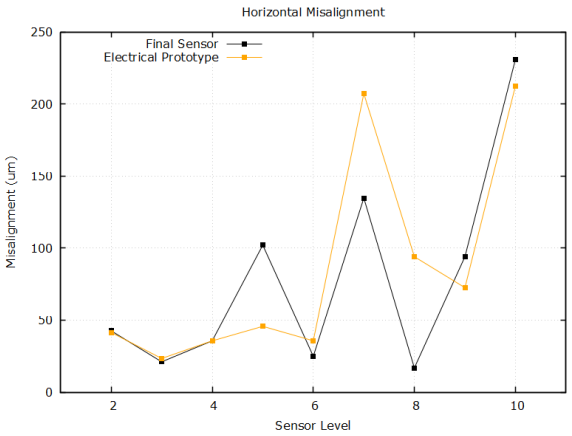

Figure 14: Horizontal Miss-alignment (Left) and Vertical Miss-alignment (Right)

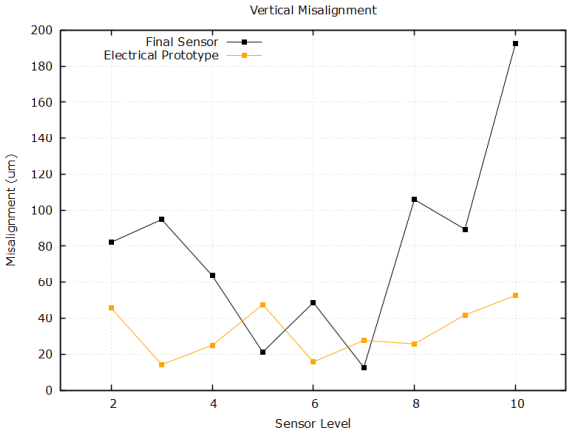

Figure 15: Horizontal Miss-alignment (Left) and Vertical Miss-alignment (Right)

Surprisingly, the results don't seem much better when using the mechanical setup for alignment. This could be from the fact that the measurements were done in a different way for the prototype, since the sample was much larger and it was hard to measure the missalignment under the microscope because of that.

A PCB containing discrete electronics was then developed and ordered online. The soldering of the electronic components was done and then the sensor was installed and wirebonding was performed, with the result shown in figure 16. Due to nanofabrication errors, it was not possible to test the whole system, since only some of the layers had functional sensors.

The final setup is shown in figure 17. The sensor installed on the PCB Board would be connected via jumpers to a micro-controller (Arduino Due) that would control the multiplexers via digital logical, thus choosing the sensors to be read. The readout signal would be amplified in the PCB and sent

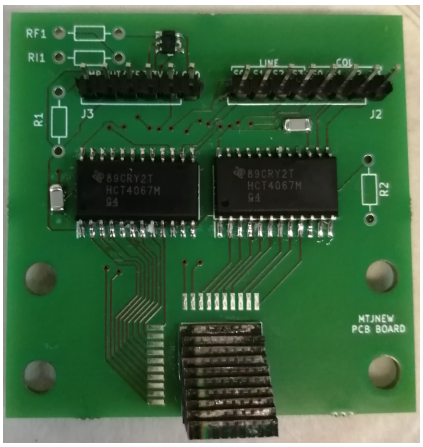

Figure 16: Final Results after PCB Assembly and Sensor Installation

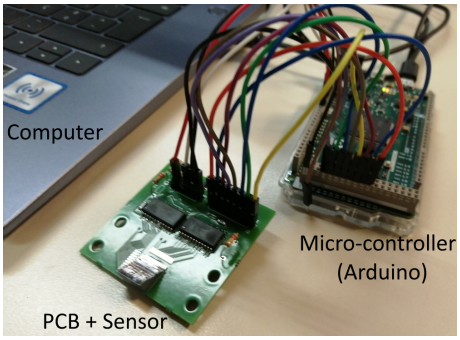

Figure 17: Final System Setup

to the computer by the microcontroller. The control of the Arduino would be done trough Matlab with the Simulink Package.

4. Results & discussion

It was not possible to obtain experimental measurements with a finished setup, therefore simulations of the expected results were produced.

The matrix fabricated of 10x10 matrix would be ideal for the mapping of 3x3 pixel matrices with resolution of approximately 3x3 sensors per pixel. Simulations for this case are shown in figure 18.

4.1. Detection Direction

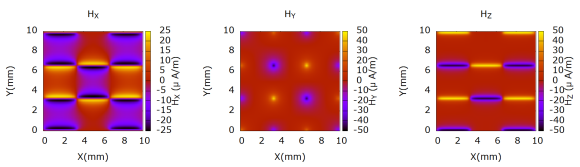

Figure 18: Mapping as a function of the Detection Direction (Magnetization X, $1cm^2$ sample, $d = 0.2mm$)

The magnetization is in the X direction, with the H_X mapping giving a mapping of the bulk of the pixels, the H_Y component giving a mapping of the corners of the pixels, while the H_Z component giving a mapping of the edges of the pixels.

As stated before, the only practical reading mode from an experimental point of view is the mapping of the magnetic field perpendicular to the magnetization. Hence, mapping of the H_Z component as a function of measuring distance was studied, with the simulations shown in figure 19.

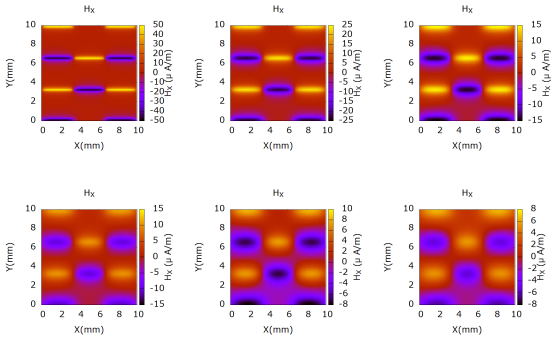

Figure 19: Perpendicular Mapping of the Edges as a function of the measuring distance

It can be observed that as the distance increases, the image becomes more blurred and the mapping of the edges becomes less defined.

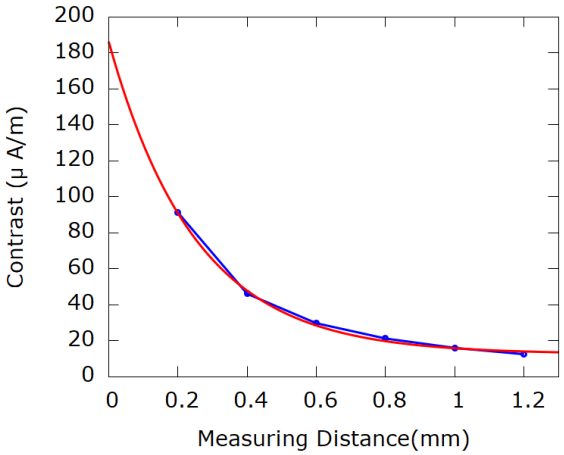

Figure 20: Mapping Contrast with Negative Exponential Fit

The algorithm that calculates the contrast is applied to the simulations to these simulations. The plots are shown in figure 20. The equations used for fitting is the following:

$$f(x) = a \cdot exp(-b \cdot x) + c \tag{5}$$

The fitting parameters are shown in table 6.

It can be observed that this model produces a good fit to the data. However, the value for the c parameter is expected to converge to zero which is not the case, for that end larger ensembles of simulations would be needed.

Parameter	a($\mu A/m$)	b(mm^{-1})	c($\mu A/m$)
Value	174 ± 10	4.0 ± 0.3	12.6 ± 1.6

Table 6: Fitting Parameters - Contrast Simulations 3x3 pixels

In order to study in more detail the interaction between neighbouring pixels, the case of a 2x2 pixel matrix ($10mm \times 10mm$) needs to be studied. For the fabricated matrix, this would correspond to a large resolution of 5×5 sensors per pixel, so the data obtained would be very reliable.

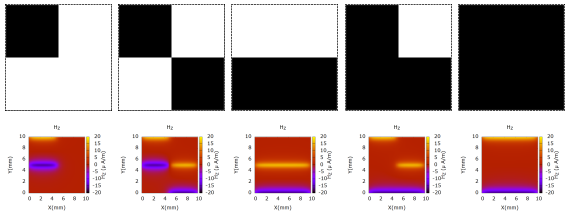

Figure 21: Possible Pixel Combinations for a 2x2 Matrix, and the perpendicular magnetic field mapping for the distance of $0.6mm$

The possible combinations of pixels are explored. For the case of 2 pixels, the case with diagonal and side-by-side positioning was studied. For the 3 and 4 pixel cases, only one meaningful arrangement is considered, since the recombinations are redundant. These combinations are shown in the figure 21.

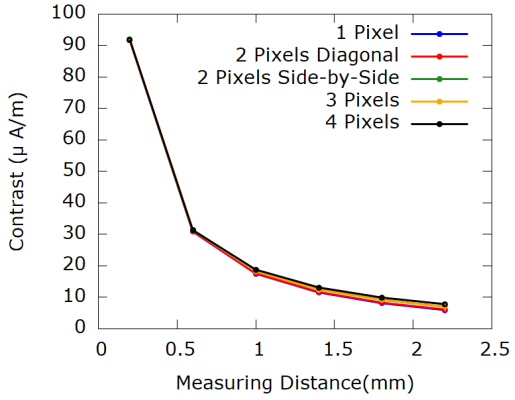

Figure 22: Contrast Plot for the different combination of pixels.

It a be observed that the contrast pattern is similar in the several combinations of pixels (fig. 22), with a divergence only occurring at larger measuring distance, where it is observed that the more pixels we have, the stronger the contrast (fig. 23).

5. Conclusions

The subject of Magnetic QR Codes is a fascinating one, since it is still very unexplored. Devices based on this technology may prove very useful for

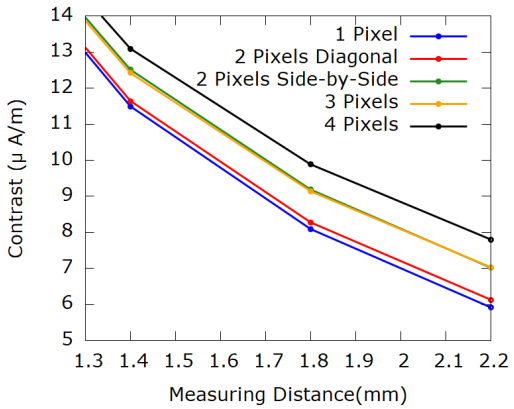

Figure 23: Contrast Plot at larger distances.

security and counterfeiting applications in the near future. They can also be used in industrial environment where optical QR Codes might not work due to deposition of surface particles. However, this is a new and emerging field, therefore there is not much previous research to start on. This provided a great opportunity to develop this thesis within this field as an answer to the needs and requests of the industry for such.

The main objective of this thesis was to prove that it is possible to read 2D magnetic patterns printed with magnetic ink and to study how parameters such as the scanning distance, number of sensors per pixel, and concentration of pixels influenced the magnetic interference between them. The first objective was clearly was clearly achieved experimentally, while the second one was done using simulations.

A simple yet effective mathematical model was employed in order to simulate the magnetic field produced by magnetic QR codes. This model was confirmed experimentally and showed how the different directions of magnetization affected the reading and then used to characterize the magnetic mapping as a function of the reading distance and the number of sensors per pixel. An algorithm for perpendicular reading was also developed for practical purposes.

The simulations of the field mapping produced by magnetic QR Codes and the results obtained from them, together with the decoding algorithm employed for perpendicular mapping represent one of the main contributions of this thesis, since the subject is very much unexplored, and no starting point was available the the beginning of the dissertation.

A novel system setup was presented: a sensor matrix consisting of layers of sensors stacked on

top of each other was proposed, together with the electronic setup to read and amplify the signals from the sensors. The required multiplexing and amplifying circuits were described.

The final layered sensor matrix was fabricated, but only partially functional. However, most of the functional sensors presented good transference curves and high percentage of magnetoresistance.

The final system setup was assembled but it was not tested due to the lack of time, as it was not expected to produce valuable useful mapping since some sensors were not working. Instead, simulations of the expected results were shown. The contrast of the mapping was studied and the results obtained showed an interesting pattern, following a negative exponential decay.

References

[1] Roger C. Palmer. *The Bar Code Book*.

[2] Denso ADC. Qr code essentials. 2011.

[3] Denso-Wave. Qr code—about 2d code. 2016.

[4] J. M. Coey. *Magnetism and magnetic materials - section 2.1.1 and 2.4*. Cambridge University Press, 2010.

[5] Kannan M. Krishnan. *Fundamentals and Applications of Magnetic Materials - section 8.7.1.4*. Oxford University Press, 2016.

[6] S. Cardoso P. Freitas, R. Ferreira and F. Cardoso. Magnetoresistive sensors. *Journal of Physics: Condensed Matter*, (19(16):165221), 2007.

[7] J. Valadeiro J. Amaral P. P. Freitas A. V. Silva, D. C. Leitao and S. Cardoso. Linearization strategies for high sensitivity magnetoresistive sensors. *The European Physical Journal Applied Physics*, (72(1):10601), 2015.

[8] R. Ferreira P. P. Freitas and S. Cardoso. Spintronic sensors. *Proceedings of the IEEE*, (104(10): 1894–1918), 2016.

[9] M. Julliere. Tunneling between ferromagnetic films. *Physics letters A*, (54(3):225–226), 1975.

[10] P. Freitas A. Guedes, M. Mendes and J. Martins. Study of synthetic ferrimagnet-synthetic antiferromagnet structures for magnetic sensor application. *Journal of applied physics*, (99(8):08B703), 2006.

[11] Sofia Alexandra Cruz Abrunhosa. Magnetoresistive sensors for industrial positioning applications. Master's thesis, Instituto Superior Técnico, 2018.

[12] J. M. Coey. *Magnetism and magnetic materials*. Cambridge University Press, 2010.

[13] Kannan M. Krishnan. *Fundamentals and Applications of Magnetic Materials*. Oxford University Press, 2016.

[14] Denso-Wave. Information capacity and versions of qr code. 2016.

[15] Orli Sharaby. Form meets function: Extreme makeover qr code edition. 2012.

[16] Russ Cox. Qart codes: How to make pictures with qr codes, part ii. 2015.

[17] Manjurul Ahsan Gupta, Kishor Datta and Stefan Andrei. Extending the storage capacity and noise reduction of a faster qr-code. *BRAIN. Broad Research in Artificial Intelligence and Neuroscience 9.1*, pages 59–71, 2018.

[18] ISO/IEC 18004:2006(E). Data encoding; table 3 – number of bits in character count indicator for qr code. 205.

[19] J. M. Coey. *Magnetism and magnetic materials - section 1.2*. Cambridge University Press, 2010.

[20] Kannan M. Krishnan. *Fundamentals and Applications of Magnetic Materials - Chapter 3*. Oxford University Press, 2016.

[21] Gustave Reed, Irving S.; Solomon. Polynomial codes over certain finite fields. *Journal of the Society for Industrial and Applied Mathematics*, 1960.

[22] W. Wesley Peterson. *Error Correcting Codes3*. MIT Press, 1961.